AIP Advances

The effect of strain and filament fracture on the transport properties of ITER cable-in-conduit conductors

Cite as: AIP Advances **10**, 065011 (2020); https://doi.org/10.1063/5.0008726
Submitted: 26 March 2020 . Accepted: 19 May 2020 . Published Online: 03 June 2020

S. Xue, P. Gao, H. Jin, G. Xiao, J. Qin, J. Li, and C. Zhou

The effect of strain and filament fracture on the transport properties of ITER cable-in-conduit conductors

Cite as: AIP Advances 10, 065011 (2020); doi: 10.1063/5.0008726
Submitted: 26 March 2020 • Accepted: 19 May 2020 •
Published Online: 3 June 2020

S. Xue,[1,2] P. Gao,[1] H. Jin,[1] G. Xiao,[1,2] J. Qin,[1] J. Li,[1,3] and C. Zhou[1,4,a)]

AFFILIATIONS

[1] Institute of Plasma Physics, Chinese Academy of Sciences, 230031 Hefei, China
[2] University of Science and Technology of China, 230026 Hefei, China
[3] Institute of Energy, Hefei Comprehensive National Science Center, 230051 Hefei, China
[4] Faculty of Science and Technology, University of Twente, Energy, Materials and Systems, 7500AE Enschede, The Netherlands

[a)] **Author to whom correspondence should be addressed:** chao.zhou@ipp.ac.cn

ABSTRACT

Dedicated experimental and modeling research studies on the performance of superconducting cable-in-conduit conductor (CICC) have been massively performed and are still ongoing in order to determine the operational limits of the conductors and to optimize their design. Strand strain distribution and crack formation in the filaments after cabling and compaction, and under cooling down and electromagnetic load have been considered as the main cause for the degradation of the CICC's transport properties. In combination with the strain maps generated by the mechanical model MULTIFIL and the electromagnetic code JackPot with the basic electrical and strain properties of the superconducting strand, the current sharing temperature (T_{cs}) of the CICC of the ITER Central Solenoid has been simulated and analyzed. A quantitative analysis of the Tcs degradation due to strain variation and filament fracture, respectively, is still missing. Here, the approach of analyzing the performance of CICC (e.g., the short samples tested in the SULTAN facility, or the full-size CICC used in real magnets) has been presented. Consequently, the effect of filament fracture on the cable T_{cs} has been investigated and turns out to be limited. Instead, the dominant mechanism behind the degradation of the transport properties of ITER type Nb_3Sn CICCs is shown to be the broadening and shift in the strain distribution of the superconducting filaments.

I. INTRODUCTION

In order to quantitatively describe the behavior of the large and complex cable-in-conduit conductor (CICCs) (e.g., the ITER magnets[1]), experiments and models have been designed and massively performed. In particular, to analyze the effects of strain in Nb_3Sn strands and multi-strand conductors, many experimental and theoretical studies,[2–15] as well as numerical cable models,[16–25] have been widely performed. As the two main causes of the degradation of CICC's transport performance, strand strain distribution and filament fracture have been investigated and analyzed.

The tests of the transport properties of ITER CICCs were carried out mainly at the SULTAN facility in Switzerland.[26] Many of the tested short cable samples show a systematic degradation of the current sharing temperature T_{cs} over several thousand current cycles under a background magnetic field of 11 T, which has been attributed mostly to filament fracture due to the electromagnetic loads on the strands.[8,26] However, detailed examination of the tested samples revealed a number of inconsistencies.[15] The proven solution for the ITER TF conductors following the TEMLOP model in solving the degradation[17,27] was adapted in favor of coupling loss reduction, allowing strand bending but with the prediction that filament fracture would remain limited. Consequently, a cable model containing sufficient strand-level details and precise strain and crack distribution in the strands of the cable is needed to quantitatively assess the influence of filament strain and crack distribution.

In this study, the coupled electromagnetic and mechanical cable models (3D strand model–MULTIFIL–JackPot) are used to quantitatively analyze the impact of strain and filament fracture on the CICC's T_{cs}. The University Twente 3D strand model predicts strand performance under different loads[28] together with the in-depth inter-filament resistance,[29] thus distinguishing the impact of strain and filament fracture on the strand performance first. The MULTIFIL model computes the strain distribution of strands imposed both by the cabling process and by the electromagnetic and thermal loads.[30] The JackPot is a numerical code for the electromagnetic network simulation of CICC, following individual strand trajectories and using measured electrical parameters between strands in CICC.[31–34]

The results of two types of crack density analyses on strands extracted from two tested ITER Central Solenoid conductor samples CSJA2-2 and CSIO1-1[35] are presented. Filament fracture is characterized post-mortem at the Applied Superconductivity Center at FSU, NHMFL (FSU), with the microscopic observation and analysis.[36] Finally, the 3D strand model[28] is applied to analyze the quantitative effect of filament cracks on the performance degradation of full-size ITER CICCs. The results indicate that the degradation of ITER Nb_3Sn CICCs can only be marginally attributed to filament fracture, but is mainly caused by the broadening and shift in the strain distribution of the superconducting filaments and corresponding inter-filamentary current redistribution.

II. CURRENT SHARING TEMPERATURE OF CICCs

The filament fracture was observed in post-mortem tested CICC samples after electromagnetic and thermal loads in the SULTAN test facility at FSU by microscopy.[36] Two such crack density analyses on strands taken from the ITER Central Solenoid conductor samples CSIO1-1 (with internal-tin strands) and CSJA2-2 (with bronze-route strands)[36] are shown in Fig. 1. They will be referred to as "crack I" [Fig. 1(a)] and "crack II" [Fig. 1(b)]. For crack II, the crack density is about a factor two lower than for crack I.

In order to evaluate the impact of cracks on the T_{cs} of the cable, the MULTIFIL strain map (Fig. 2) for the cable with the CSIO Baseline design[13,30] and the directly observed crack distribution at FSU[36] are combined. The measurement of T_c of CICC shows similar strain distribution and average axial strain from Ciro Calzolaio.[37] The average strand neutral-axis axial strain (ε_{a0}) in the CSIO1 conductor is about −0.4%, while the peak periodic bending strain (ε_{pb}) in the multi-filamentary region is around 0.6%.[30]

These estimates are validated by comparing the voltage vs current (V–I) curve of a single strand simulated with the 3D strand model[28] for $\varepsilon_{a0} = -0.4\%$ and $\varepsilon_{pb} = 0.6\%$ with the JackPot cable model predictions for the strand that experiences the most severe strain condition in the MULTIFIL map. Both simulations assume the temperature and external magnetic field corresponding to a cable test in SULTAN.

All relevant test conditions, temperature, magnetic field, ε_{a0}, and ε_{pb}, together with the results of the filament fracture analysis at FSU, can now be introduced into the strand model to evaluate the relative impact of cracks on the cable performance.

In order to identify the impact of different crack scenarios (cracks I and II) on the V–I transition of the strands and on their

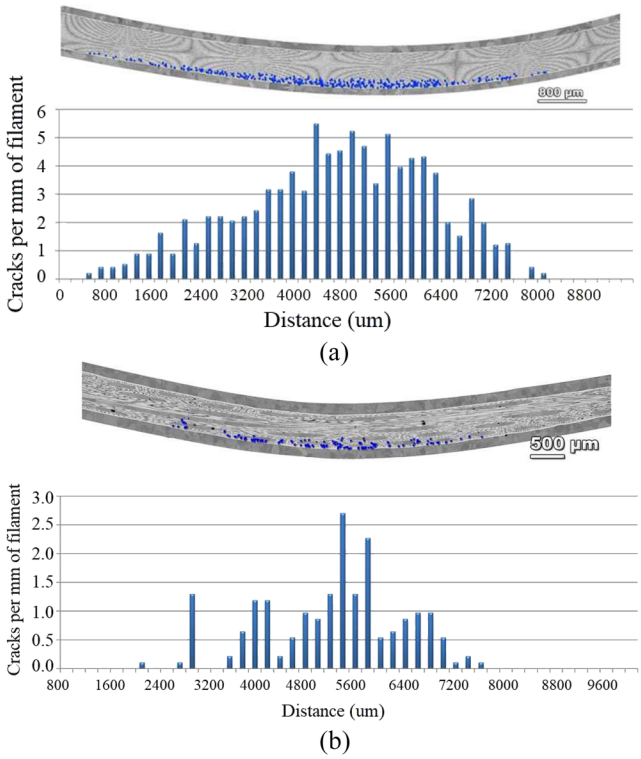

FIG. 1. (a) A polished longitudinal section of a CSIO1-1 internal-tin strand with cracks indicated by blue dots. The location suggests tensile bending strain. (b) The corresponding crack density, expressed in number of cracks per mm of filament length for CSJA2-2 (courtesy of C. Sanabria, FSU, now at LBL).[36] Distance in the axis indicates the location along the sample length.

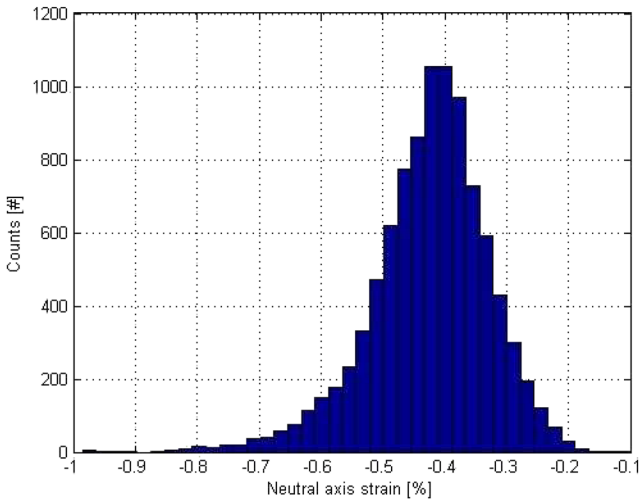

FIG. 2. Number of the strand neutral-axis axial strain present in the CSIO Baseline cable design as calculated with the MULTIFIL model (courtesy of H. Bajas, Ecole Centrale Paris, now at CERN).

critical current I_c, the modeling approach is repeated by implementing the observed crack density and distribution into the strand model. The strain boundary conditions correspond to a ε_{pb} value of +0.6% and a ε_{a0} value of −0.4% for the internal-tin strand in the CSIO1-1 sample. For the bronze-route strand, no MULTIFIL strain map is yet available, but from the large difference in axial stiffness, a corresponding ε_{pb} value of at least +0.8% may be expected for this strand, while the neutral-axis axial strain is taken to be the same $\varepsilon_{a0} = -0.4\%$.

The V–I curve corresponding to scenario crack I is compared to the one of a crack-free bronze-route strand, while scenario crack II is compared to a crack-free internal-tin strand. The results are shown in Figs. 3 and 4, respectively. In the bronze-route strand, cracks induce a much stronger critical current degradation than in the internal-tin wire. This is partly due to the higher crack density in the crack I scenario, but also to bridging that couples most filaments in each bundle in the internal-tin strand.

Assuming that each strand has the same crack density and distribution along the tested cable, the ITER scaling law can be used to estimate the reduction in T_{cs} caused by filament fracture, as shown in Fig. 5. From the analysis in Ref. 36, it can be deduced that each strand experiences only one location with crack II conditions in the 0.5 m long CSIO1-1 cable; the reduction in T_{cs} is less than 40 mK. For cable CSJA2-2 with bronze-route strands and fracture scenario crack I, it amounts to 120 mK. Figure 7 also shows the impact of a much larger amount of cracks even assuming cracks along the entire strand. Following this analysis, in this extreme case, reductions in T_{cs} of around 1.7 K and 0.6 K can be expected for the CSJA2-2 and CSIO1-1 conductors, respectively.

The bronze-route strand is also modeled with crack I scenario at different values of peak bending strain (Fig. 6). At a higher peak bending strain, filament fracture has a lower impact on T_{cs}. For the same crack pattern, a higher peak bending strain implies that the fractured filaments already have a lower I_c value so that a crack causes less current redistribution and the impact of cracks on T_{cs} is reduced.

The simulations presented in Fig. 7 predict a decrease in T_{cs} of 120 mK due to scenario crack I and 40 mK due to scenario crack II for a bronze-route strand. With the extreme assumption of the crack I scenario occurring every 7 mm or the crack II scenario occurring once every 5 mm along the strand, a T_{cs} reduction of 1.7 K or 1.1 K may occur, respectively. The filament fracture analysis at FSU

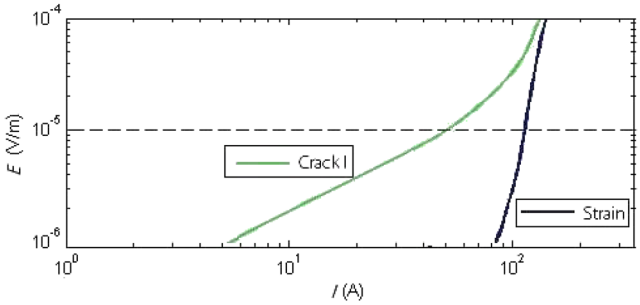

FIG. 3. Electrical-field vs current expected for the filament fracture scenario crack I (green curve), compared to a bronze-route strand with only a strain distribution (blue curve, $\varepsilon_{a0} = -0.4\%$ and $\varepsilon_{pb} = 0.8\%$).

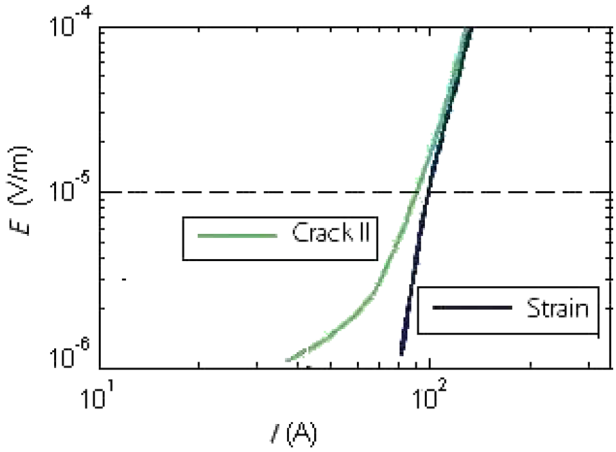

FIG. 4. Electrical-field vs current relation expected for the filament fracture scenario crack II (green curve), compared to an internal-tin strand with only a strain distribution (blue curve, $\varepsilon_{a0} = -0.4\%$ and $\varepsilon_{pb} = 0.6\%$).

revealed no evidence of cracks when the tensile strain remains below 0.8%. Based on the crack analysis in CSJA2-2 and in the TARSIS-bent bronze-route strands,[38] the ε_{pb} value in the CSJA2-2 conductor is higher than 1.0%. Therefore, the impact of cracks should be even less than in the $\varepsilon_{pb} = 1.0\%$ simulation shown in Fig. 4. Even in the extreme case (see Fig. 8), so for strands with the crack I scenario every 7 mm along the entire cable, the T_{cs} reduction caused by the crack I scenario would be less than 1.7 K ($\varepsilon_{pb} = 0.8\%$), and more likely below 0.6 K ($\varepsilon_{pb} = 1.0\%$). Normally, however, each strand is expected to exhibit only one crack I or crack II event along the 0.5 m cable and the T_{cs} reduction caused by cracks in CSIO1-1 and CSJA2-2 conductors most likely lies in the range of 0.04–0.12 K. The T_{cs} of ITER Nb_3Sn CICC seems to degrade mainly due to local strain variation, rather than to filament fracture, which also has been concluded similarly in the research from FSU.[39]

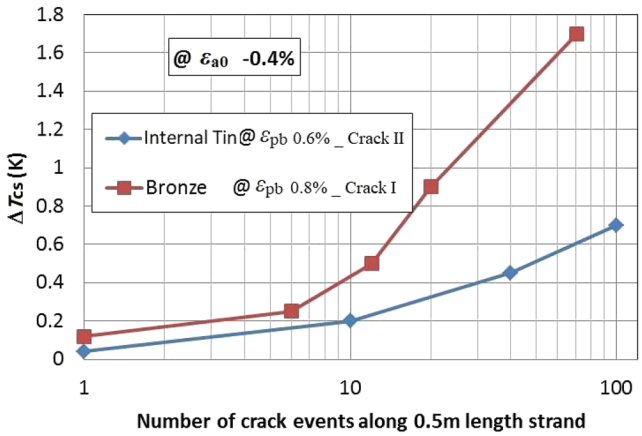

FIG. 5. Change in T_{cs} (ΔT_{cs}) vs number of cracks, showing the impact of filament fracture on T_{cs} in a 0.5 m long conductor with a strain condition based on MULTIFIL and TARSIS. Both bronze-route and internal-tin strands are modeled with crack I and crack II scenarios, respectively.

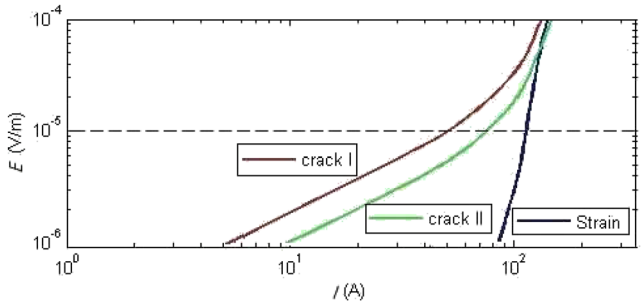

FIG. 6. Electrical-field vs current relation expected for filament fracture crack I and crack II scenarios (brown and green curves), compared to a bronze-route strand subjected to only a strain distribution (blue curve, ε_{a0} = −0.4% and ε_{pb} = +0.8%).

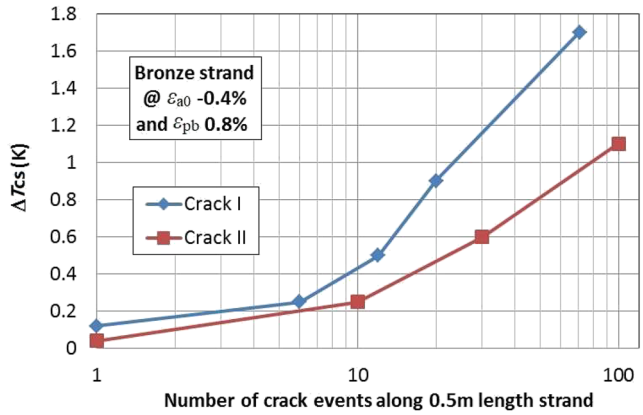

FIG. 7. ΔT_{cs} vs number of cracks showing the impact of filament fracture scenarios crack I and crack II on the T_{cs} reduction in a 0.5 m long bronze-route conductor with strain conditions based on MULTIFIL and TARSIS.

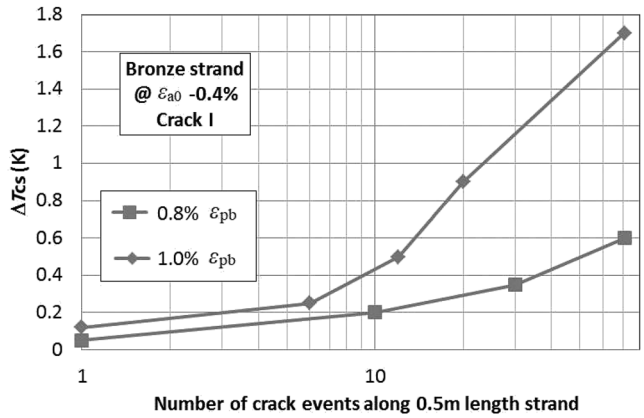

FIG. 8. ΔT_{cs} vs number of cracks showing the impact of filament fracture scenario crack I on the T_{cs} reduction in a 0.5 m long bronze-route conductor with strain conditions based on MULTIFIL and TARSIS and peak bending strain ε_{pb} = +0.8% or +1.0%.

III. CONCLUSION

The crack distribution is based on a microscopy analysis of strands from post-mortem full-size ITER conductor samples. Given the amount of filament fracture observed in post-mortem TARSIS and full-size ITER samples, the 3D strand model effectively quantifies the impact of cracks on the strand and the final CICC performance. The impact of filament fracture on the T_{cs} of the investigated cables is found rather limited. Even for a crack frequency 10 times higher than the one observed in full-size ITER samples after loading, the reduction in T_{cs} remains less than 0.2 K. It is concluded that the transport properties of ITER Nb_3Sn CICCs mainly degrade due to the broadening and shift in the strain distribution of the superconducting filaments and corresponding inter-filamentary current redistribution, rather than to filament fracture.

ACKNOWLEDGMENTS

This work was supported by the 2019 National Key Research and Development Plan, Grant No. 2019YFC0117502, and the National High Level Research Project. The authors thank C. Sanabria, P. Lee, and D. Larbalestier from Florida State University for the useful discussions and providing the microscopic observed data and plots of filament fracture from the cable. We also thank H. Bajas (Ecole Centrale Paris) and A. Devred (ITER) for supporting the mechanical modeling with MULTIFIL (now both of them work at CERN, Switzerland).

Data AVAILABILITY

The data that support the findings of this study are available from the corresponding author upon reasonable request.

REFERENCES

[1] A. Nijhuis *et al.*, "The effect of axial and transverse loading on the transport properties of ITER Nb_3Sn strands," Supercond. Sci. Technol. **26**, 084004 (2013).
[2] N. Mitchell, "Operating strain effects in Nb_3Sn cable-in-conduit conductors," Supercond. Sci. Technol. **18**, S396 (2005).
[3] N. C. Van den Eijnden, A. Nijhuis, Y. Ilyin, W. A. J. Wessel, and H. H. J. ten Kate, "Axial tensile stress–strain characterization of ITER model coil type Nb_3Sn strands in TARSIS," Supercond. Sci. Technol. **18**, 1523–1532 (2005).
[4] M. C. Jewell, P. J. Lee, and D. C. Larbalestier, "The influence of Nb3Sn strand geometry on filament breakage under bend strain as revealed by metallography," Supercond. Sci. Technol. **16**, 1005 (2003).
[5] D. Ciazynski, "Review of Nb_3Sn conductors for ITER," Fusion Eng. Des. **82**, 488–497 (2007).
[6] N. Mitchell, "Assessment of conductor degradation in the ITER CS insert coil and implications for the ITER conductors," Supercond. Sci. Technol. **20**, 25–34 (2007).
[7] D. Bessette, "Sensitivity of Nb_3Sn ITER conductor design to selected parameters," IEEE Trans. Appl. Supercond. **13**, 1433–1436 (2003).
[8] P. Bruzzone *et al.*, "Test results of two ITER TF conductor short samples using high current density Nb_3Sn strands," IEEE Trans. Appl. Supercond. **17**, 1370–1373 (2007).
[9] A. Nijhuis *et al.*, "Impact of void fraction on mechanical properties and evolution of coupling loss in ITER Nb_3Sn conductors under cyclic loading," IEEE Trans. Appl. Supercond. **15**, 1633–1636 (2005).
[10] A. Nijhuis *et al.*, "Optimization of interstrand coupling loss and transverse load degradation in ITER Nb_3Sn CICCs," IEEE Trans. Appl. Supercond. **23**, 64–69 (2013).

[11] D. P. Boso, M. Lefik, and B. A. Schrefler, "Thermal and bending strain on Nb_3Sn strands," IEEE Trans. Appl. Supercond. **16**, 1823–1826 (2006).
[12] D. P. Boso, M. J. Lefik, and B. A. Schrefler, "Thermo-mechanics of the hierarchical structure of ITER superconducting cables," IEEE Trans. Appl. Supercond. **17**, 1362–1365 (2007).
[13] H. Bajas *et al.*, "Approach to heterogeneous strain distribution in cable–in-conduit conductors through finite element simulation," IEEE Trans. Appl. Supercond. **22**, 4803104 (2012).
[14] T. Wang, L. Chiesa, and M. Takayasu, "Fundamental simulations of transverse load effects on Nb_3Sn strands using finite element analysis," AIP Conf. Proc. **1435**, 243 (2012).
[15] A. Devred, C. Jong, and N. Mitchell, "Strain redistribution effects on current-sharing measurements on straight samples of large Nb_3Sn cable-in-conduit conductors," Supercond. Sci. Technol. **25**, 054009 (2012).
[16] N. Mitchell, "Analysis of the effect of Nb_3Sn strand bending on CICC superconductor performance," Cryogenics **42**, 311–325 (2002).
[17] A. Nijhuis and Y. Ilyin, "Transverse load optimisation in Nb_3Sn CICC design; influence of cabling, void fraction and strand stiffness," Supercond. Sci. Technol. **19**, 945–962 (2006).
[18] R. Zanino *et al.*, "Coupled mechanical–electromagnetic–thermal–hydraulic effects in Nb_3Sn cable-in-conduit conductors for ITER Supercond," Sci. Technol. **18**, S376 (2005).
[19] N. Koizumi, Y. Nunoya, and K. Okuno, "A new model to simulate critical current degradation of a large CICC by taking into account strand bending," IEEE Trans. Appl. Supercond. **16**, 831–834 (2006).
[20] N. Mitchell, "Comparison between predictions and measurements of the superconducting performance of Nb_3Sn cable," Supercond. Sci. Technol. **21**, 054015 (2008).
[21] Y. Zhai and M. D. Bird, "Florida electro-mechanical cable model of Nb_3Sn CICCs for high-field magnet design," Supercond. Sci. Technol. **21**, 115010 (2008).
[22] A. Torre *et al.*, "Mechanical-electrical modeling of stretching experiment on 45 Nb_3Sn strands CICCs," IEEE Trans. Appl. Supercond. **21**, 2042–2045 (2011).
[23] M. Breschi *et al.*, "Modeling of the electro-mechanical behavior of ITER Nb_3Sn cable in conduit conductors," Supercond. Sci. Technol. **25**, 054005 (2012).
[24] T. Bajas, L. Chiesa, and M. Takayasu, "Finite element analysis of Nb_3Sn subcables under transverse compression with different approaches," IEEE Trans. Appl. Supercond. **23**, 8400705 (2013).
[25] Y. Zhai, "Electro-mechanical modeling of Nb_3Sn CICC performance degradation due to strand bending and inter-filament current transfer," Cryogenics **50**, 149–157 (2010).
[26] P. Bruzzone *et al.*, "Upgrade of operating range for SULTAN test facility," IEEE Trans. Appl. Supercond. **12**, 520–523 (2002).
[27] A. Nijhuis *et al.*, "A solution for transverse load degradation in ITER Nb_3Sn CICCs: Verification of cabling effect on Lorentz force response," Supercond. Sci. Technol. **21**, 054011 (2008).
[28] Y. Miyoshi *et al.*, "Modelling of current distribution in Nb_3Sn multifilamentary strands subjected to bending," Supercond. Sci. Technol. **25**, 054003 (2012).
[29] C. Zhou *et al.*, "Inter-filament resistance, effective transverse resistivity and coupling loss in superconducting multi-filamentary NbTi and Nb_3Sn strands," Supercond. Sci. Technol. **25**, 015013 (2012).
[30] H. Bajas, "Numerical simulation of the mechanical behavior of the ITER cable-in-conduit conductors," Ph.D. thesis, Ecole Centrale de Paris, 2012.
[31] E. P. A. van Lanen and A. Nijhuis, Cryogenics **50**, 139 (2009).
[32] E. P. A. van Lanen and A. Nijhuis, "Numerical analysis of the DC performance of ITER TF samples with different cabling pattern based on resistance measurements on terminations," Supercond. Sci. Technol. **24**, 085010 (2011).
[33] E. P. A. van Lanen and A. Nijhuis, "Simulation of interstrand coupling loss in cable-in-conduit conductors with JackPot-AC," IEEE Trans. Appl. Supercond. **21**(3), 1926–1929 (2011).
[34] G. Rolando, "Cable-in-conduit superconductors for fusion magnets," Ph.D. thesis, University of Twente, 2013.
[35] A. Devred *et al.*, "Status of ITER conductor development and production," IEEE Trans. Appl. Supercond. **23**, 6464523 (2013).
[36] C. Sanabria *et al.*, *Presentation: Quantifying Filament Fractures in Nb_3Sn Composite Strands for Modeling Purposes* (Florida State University, 2013).
[37] C. Calzolaio, "Irreversible degradation in Nb_3Sn cable in conduit conductors," Ph.D. thesis, EPFL SPC, 2013.
[38] A. Nijhuis *et al.*, "Impact of spatial periodic bending and load cycling on the critical current of a Nb_3Sn strand," Supercond. Sci. Technol. **18**, S273–S283 (2005).
[39] C. Eijnden, P. J. Lee, W. Starch, A. Devred, and D. C. Larbalestier, "Metallographic autopsies of full-scale ITER prototype cable-in-conduit conductors after full cyclic testing in SULTAN: III. The importance of strand surface roughness in long twist pitch conductors," Supercond. Sci. Technol. **29**(7), 074002 (2016).